Superhydrophobic and Superoleophilic Porous Boron Nitride Nanosheet/Polyvinylidene Fluoride Composite Material for Oil-Polluted Water Cleanup

Yuanlie Yu, Hua Chen, Yun Liu, Vincent S. J. Craig, Chunming Wang, Lu Hua Li, and Ying Chen*

Oily wastewater generated from various manufacturing industries, including petrochemical, food, textiles, leather, and metallurgical industries as well as from frequent oil spills, has become a very serious environmental issue.[1] The insoluble oil could decompose to other harmful chemicals further polluting the natural environment and threatening aqueous habitats and affecting human health.[2] Till now, it is still a worldwide challenge on how to cleanse the oil from such polluted water. Traditional methods for treating oil-polluted water includes oil skimmers, centrifuges, coalesces, settling tanks, depth filters, magnetic separations, flotation technologies, oil-absorbing materials, and ignition of the oil.[3] However, more stringent environmental controls and the pressure of economic development has led to a desire to produce more effective processes. Recently, a new type of material with superhydrophobic and superoleophilic or superhydrophilic and superoleophobic features has attracted considerable attention. These materials, such as polyvinylidene fluoride (PVDF) membranes,[3a,4] boron nitride nanotubes-coated stainless steel meshes,[5] titanium oxide-coated copper meshes,[6] cuprous oxide-coated copper meshes,[7] marshmallow-like gels,[8] polytetrafluoroethylene (PTFE)-coating meshes,[9] trichloromethylsilane-coated polyester textiles,[10] nanoporous polydivinylbenzene materials,[11] cross-linked oil-absorbing polymer gels,[12] and carbonaceous nanofiber hydrogels and Aerogels,[13] pumping-assisted porous hydrophobic/oleophilic materials,[14] can simply and efficiently separate oil from water either by filtration or absorption of oil from the mixtures. Based on these pioneering works, it is important to develop novel materials for oil/water separation that result in a good separation efficiency, high stability, and recyclability.

PVDF-based materials are attractive for fabricating microfiltration and ultrafiltration membranes to separate oil and water due to their outstanding thermal stability, chemical resistance, and high mechanical strength.[15] PVDF membranes fabricated by the hot-press approach (with a skin layer) are hydrophilic, exhibiting contact angles (CAs) less than 90°,[16] therefore other techniques have been sought to make PVDF surfaces hydrophobic or even superhydrophobic. Zhang et al.[3a] found that the PVDF membranes fabricated by a modified-phase inversion approach are superhydrophobic and superoleophilic. Such PVDF membranes can be used to effectively separate a wide range of water-in-oil emulsions including surfactant-free and surfactant-stabilized emulsions with droplet sizes from micrometer to nanometer range with a high-separation efficiency (>99.95%) even at an extremely high flux. Zha et al.[17] also demonstrated that hydrophobic PVDF porous materials (water CA: 135.8°) can be achieved by a slow solvent-exchange and subsequent freeze-drying method. The water-repellent property of such porous PVDF materials can be further improved by adding a small amount of graphene (1 wt%).[17] The addition of graphene in the PVDF gels can lead to morphological changes by influencing the crystallization of PVDF to form porous PVDF materials with rough surfaces, resulting in the superhydrophobicity. These studies indicate that the surface wettability of PVDF materials can be dramatically reduced by special fabrication processes and the addition of other fillers.

Structurally, similar to graphene, hexagonal boron nitride nanosheets (*h*-BNNSs) also possess remarkable mechanical properties and thermal conductivity.[18] Moreover, *h*-BNNSs exhibit high chemical inertness and thermal stability, excellent resistance to oxidation, and good optical properties in comparison to graphene as well as a constant wide bandgap (5–6 eV).[19] These make *h*-BNNSs an extremely attractive additive to insulating composites where strong mechanical properties and excellent thermal conductivity in harsh environments are required.[20]

Here, we report on the fabrication by a phase inversion process of a novel porous composite material that makes use of the unique properties of *h*-BNNSs and the hydrophobicity and oleophilicity of PVDF. The other advantage of chosing BNNSs as the filler is that they can easily be scaled-up produced and are

Dr. Y. Yu, Dr. H. Chen
Centre for Advanced Microscopy
Australian National University
Canberra, ACT 0200, Australia
E-mail: hua.chen@anu.edu.au
Prof. Y. Liu, Dr. C. Wang
Research School of Chemistry
Australian National University
Canberra, ACT 0200, Australia
Prof. V. S. J. Craig
Department of Applied Mathematics
Research School of Physics and Engineering
Australian National University
Canberra, ACT 0200, Australia
Dr. L. H. Li, Prof. Y. Chen
Institute for Frontier Materials
Deakin University
Geelong Waurn Ponds Campus
VIC 3216, Australia

DOI: 10.1002/admi.201400267

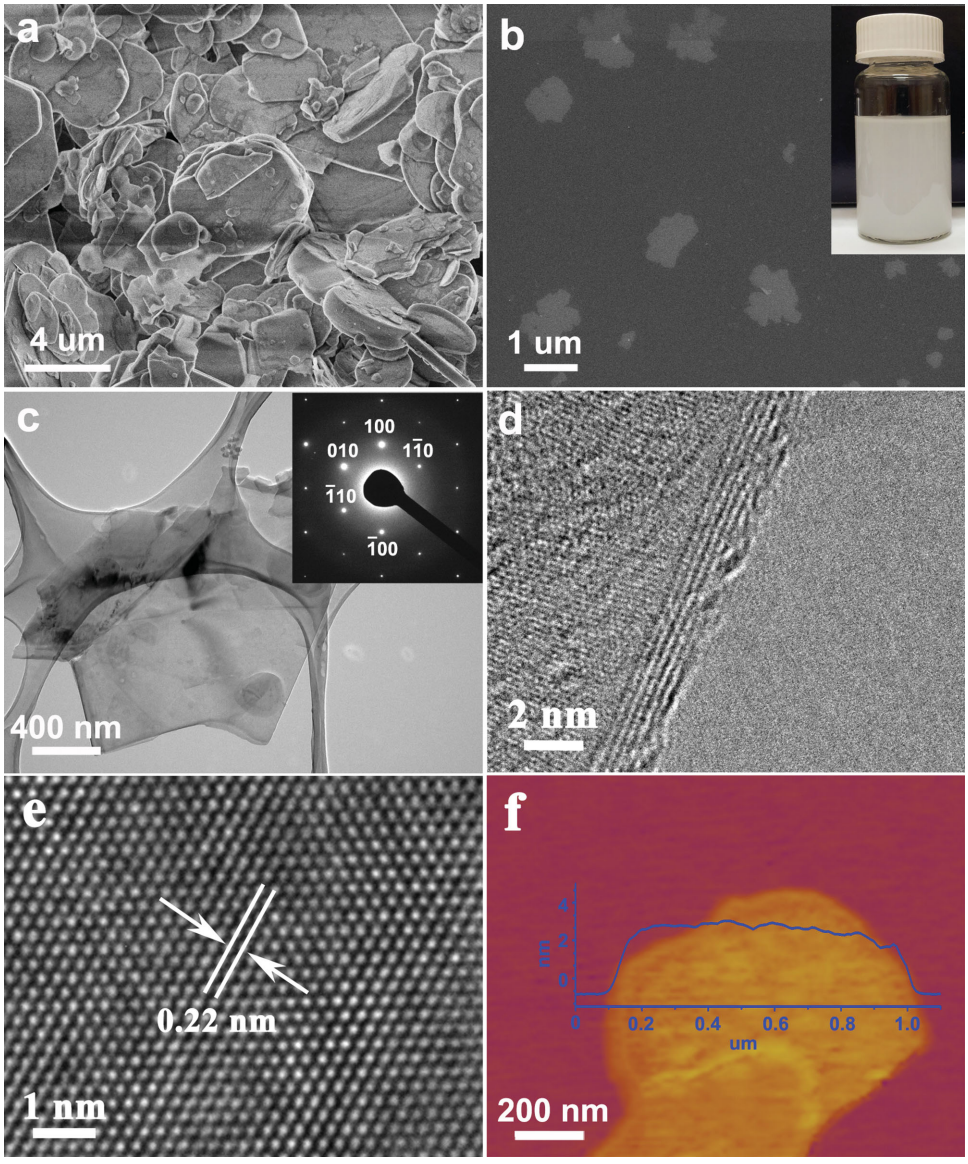

Figure 1. FESEM, TEM, HRTEM, and AFM analysis of the precursor and exfoliated BNNSs: a) FESEM image of bulk *h*-BN, b) FESEM image of exfoliated BNNSs, the inset is a photograph of exfoliated BNNSs dispersed in IPA standing for one month, c) TEM images of exfoliated few-layered *h*-BNNSs and corresponding SAED pattern d) HRTEM image of the BNNS with 5-layer BN, e) HRTEM image of BNNS, and f) AFM image and the corresponding height trace of a *h*-BNNS.

therefore cheaper and easier to use.[21] In order to characterize the novel porous BNNS/PVDF composite material, the hydrophobicity and oleophilicity was examined by measuring static water and oil CAs and the material properties characterized using a range of microscopies and analytical techniques. The selectivity and efficiency of the porous BNNS/PVDF composite material as a membrane and absorbent for oil/water separation was investigated. In addition, the durability, stability, and recyclability of the composite were examined.

It is well known that the large *h*-BNNSs result in more efficient reinforcement in mechanical strength and thermal conductivity.[22] Thus, in order to extract the larger fraction of *h*-BNNSs two centrifugation steps were employed during the separation process.[23] The first step was to separate the thin *h*-BNNSs from the thicker unexfoliated *h*-BN particles at a rotation speed at 1000 rpm (Figure S1, Supporting Information). However, nanoscaled BN particles and flakes are still present with the thin *h*-BNNSs in the supernatant collected from the first centrifugation. The second step is to remove these nanoscaled particles and flakes from the thin *h*-BNNSs by further centrifugation the collected supernatant at a higher speed of 10 000 rpm. Thin *h*-BNNSs of relatively large sizes could be obtained by washing the sediment after the second centrifugation step by ethanol and subsequently drying at 60 °C and used as the filler material for porous BNNS/PVDF composite material fabrication.

Figure 1a,b presents the field emission scanning electron microscope (FESEM) images of the starting *h*-BN particles

and the thin *h*-BNNSs after exfoliation and two-step centrifugation. The *h*-BN precursors exhibit irregular shapes with lateral sizes ranging from hundreds of nanometers to several micrometers and thickness ranging from tens of nanometers to about 1 µm. Figure 1b shows a high-magnification FESEM image of the thin *h*-BNNSs. Clearly, compared with the starting *h*-BN, both the lateral size and thickness of the exfoliated products are decreased. The inset in Figure 1b is a photograph of the exfoliated *h*-BNNSs dispersed in isopropanol (IPA), exhibiting a milky white color. It is noteworthy that these dispersions are homogenous and stable. Figure 1c shows a transmission electron microscope (TEM) image and corresponding selected area electron diffraction pattern (SAED, inset in Figure 1c) of the *h*-BNNSs. In contrast to the *h*-BN particles, *h*-BNNSs have a small thickness and are nearly transparent to the electron beam. The lateral sizes of the *h*-BNNS are also reduced compared to the *h*-BN. The corresponding SAED pattern exhibits the characteristic sixfold diffraction symmetry for *h*-BN, suggesting the *h*-BNNSs are highly crystalline, which can be further confirmed by HRTEM study. As shown in Figure 1e, the hexagonal lattice structure of the *h*-BNNSs can be seen, in which the marked white line shows the measured d-spacing of 0.22 nm, nearly equaling to the distance of the (100) planes of *h*-BN.[24] Similar to graphene, the edges of the *h*-BNNSs are prone to be folded, which allows us to directly measure the number of layers by HRTEM. A typical five-layered *h*-BNNS with a thickness of about 1.67 nm is shown in Figure 1d. This corresponds to a layer separation of 0.334 nm, which is close to the intrinsic (002) plane spacing of *h*-BN (0.3328 nm).[24] In fact, most of the *h*-BNNSs consisted of less than ten layers, as demonstrated by TEM (Figure S2, Supporting Information). Furthermore, the thickness of the *h*-BNNS can also be estimated from atomic force microscopy (AFM) images. Based on the AFM measurements on a large number of *h*-BNNSs, it was found that the surfaces of these sheets are rather flat and nearly all the *h*-BNNSs are thin sheets with thicknesses less than 5 nm. This is consistent with the TEM analysis (Figure 1f). More importantly, in the ultrasonication process, no other functional groups, such as hydroxyl and alkyl, were introduced into the *h*-BNNSs (Figure S3, Supporting Information), suggesting that they will maintain the excellent properties of pure *h*-BNNSs.

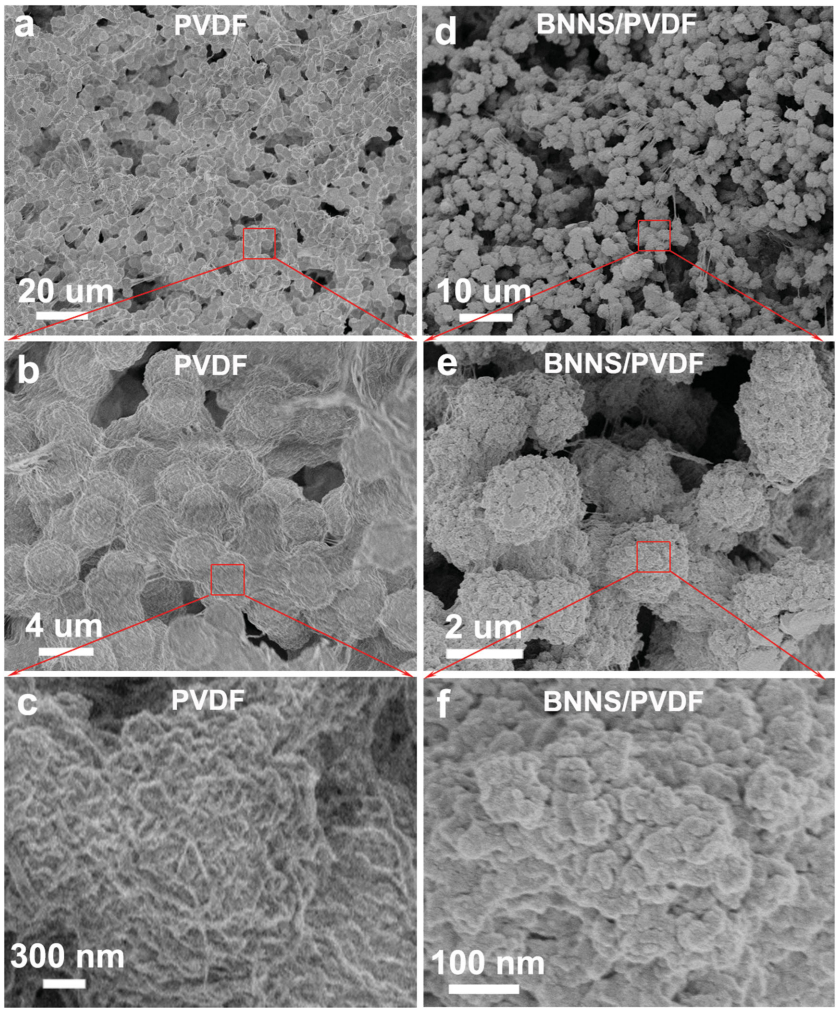

Figure 2. a–c) The FESEM images of the PVDF and d–f) porous BNNS/PVDF composite material.

Figure 2a,d exhibits FESEM images of large area views of the pure PVDF and porous BNNS/PVDF composite material, respectively. Both the materials have porous structures and rough surfaces. However, compared with the pure PVDF, the porous BNNS/PVDF composite material possesses more and larger pores. The enlarged FESEM images (Figure 2b,e) reveal that these holes are formed by stacking of spherical microparticles. For the porous BNNS/PVDF composite material, the diameter of spherical microparticles is 1–3 µm (Figure 2e) that is smaller than the pure porous PVDF microparticles, which are in the range of 3–6 µm (Figure 2b). Noticeably, the surfaces of these microparticles are not smooth, but have micro- and nanoscale protrusions distributed on the surface. Nevertheless, the surface of the spherical microparticles composed of pure PVDF forms cellular nanostructures which densely stack together, as shown in Figure 2c. In contrast, the surface of the spherical microparticles composed of porous BNNS/PVDF composite material is constituted of nanoparticles which are loosely assembled (Figure 2f). The existence of such loose nanoparticles dramatically increases the surface roughness of the porous BNNS/PVDF composite material. On the basis of the previous studies, the difference in morphology originates from different formation mechanisms. The formation of physical gels is typically dominated by the cooperative effects of liquid--liquid demixing and solid–liquid demixing (or the crystallite formation of polymer chains).[25] Zha et al.[17] found that the cellular nanostructure is formed via liquid–liquid demixing, whereas the assembly of nanospheres is promoted

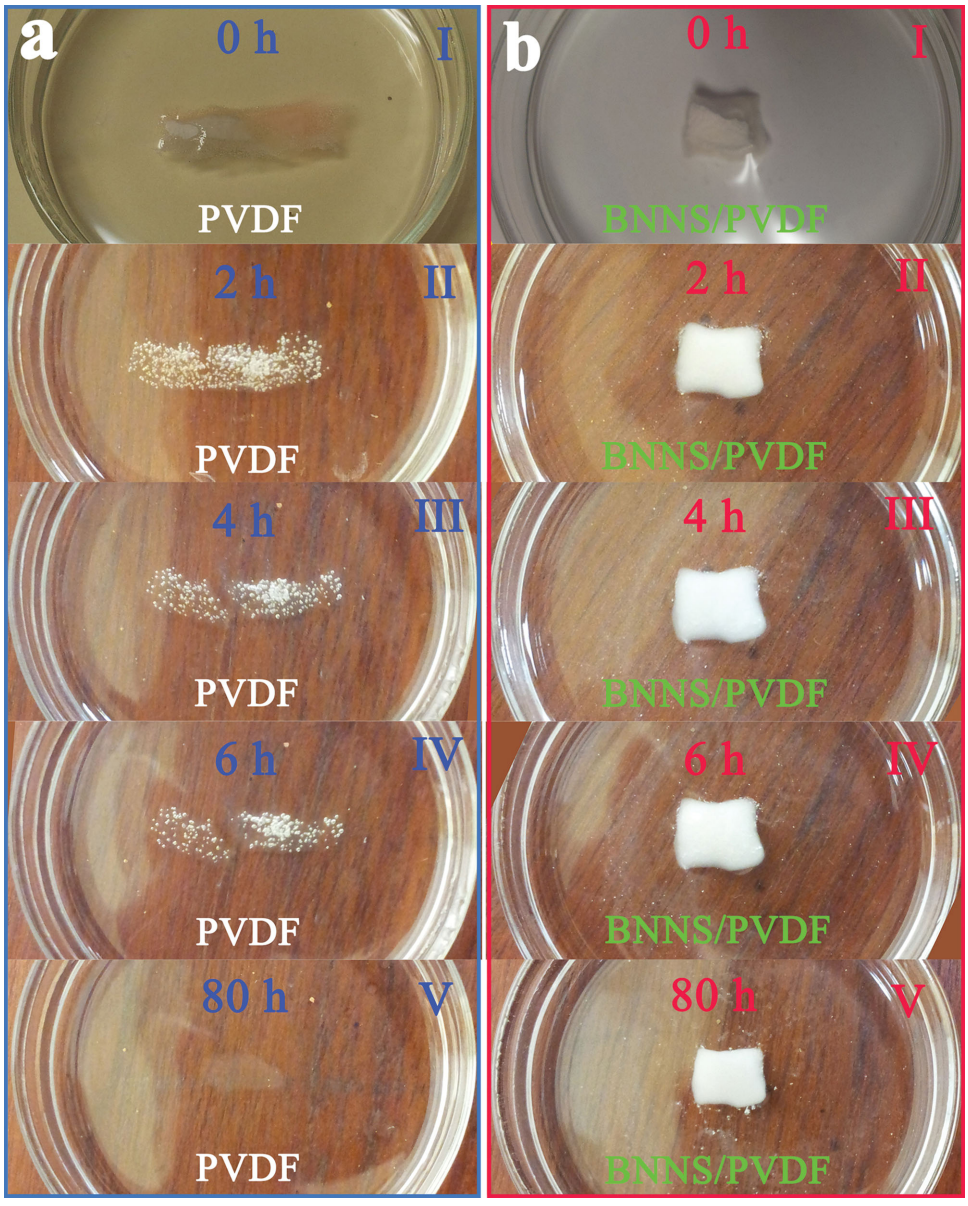

Figure 3. Photographs of pure PVDF a) and porous BNNS/PVDF composite materials b) dissolved in DMF for 80 h.

by a solid–liquid demixing process. In the current case, the formation mechanisms of porous PVDF and porous BNNS/PVDF composite materials are similar to those described by Zha et al., in which the porous PVDF material forms via a liquid–liquid demixing process while the porous BNNS/PVDF composite material forms by a solid–liquid demixing, where *h*-BNNSs can act as crystallization nuclei, thus promoting solid–liquid demixing. So it can be concluded that the addition of *h*-BNNSs into PVDF does not only change the pore size and surface morphology but also influences the crystallization.

Note that the addition of *h*-BNNSs could improve the stability of PVDF materials. To evaluate this, equal amounts (0.1245 g) of pure PVDF and porous BNNS/PVDF composite materials were placed into N, N-dimethylformamide solvent (DMF) to evaluate the solubility. As shown in **Figure 3**, most of the pure PVDF dissolved in DMF after 80 h, but only a minute portion of the porous BNNS/PVDF composite material dissolved at the same time. Moreover, such porous BNNS/PVDF composite material can even be kept for more than 2 weeks in DMF without being dissolved (Figure S4, Supporting Information). It is well known that large-area 2D BNNSs can fully exhibit the unique properties of (002) sp^2-hybridized crystal planes. Moreover, their large specific surface area can further prolong interactional interfaces and intensifies interfacial interaction between BN and polymer molecules, forming diverse functionally reinforced plastics, thus improving the stability of the composite material.[26] Additionally, changes to the surface morphology and increases in the surface roughness of porous BNNS/PVDF composite material induced by the introduction of *h*-BNNSs could also lead to the alteration of surface properties, such as surface

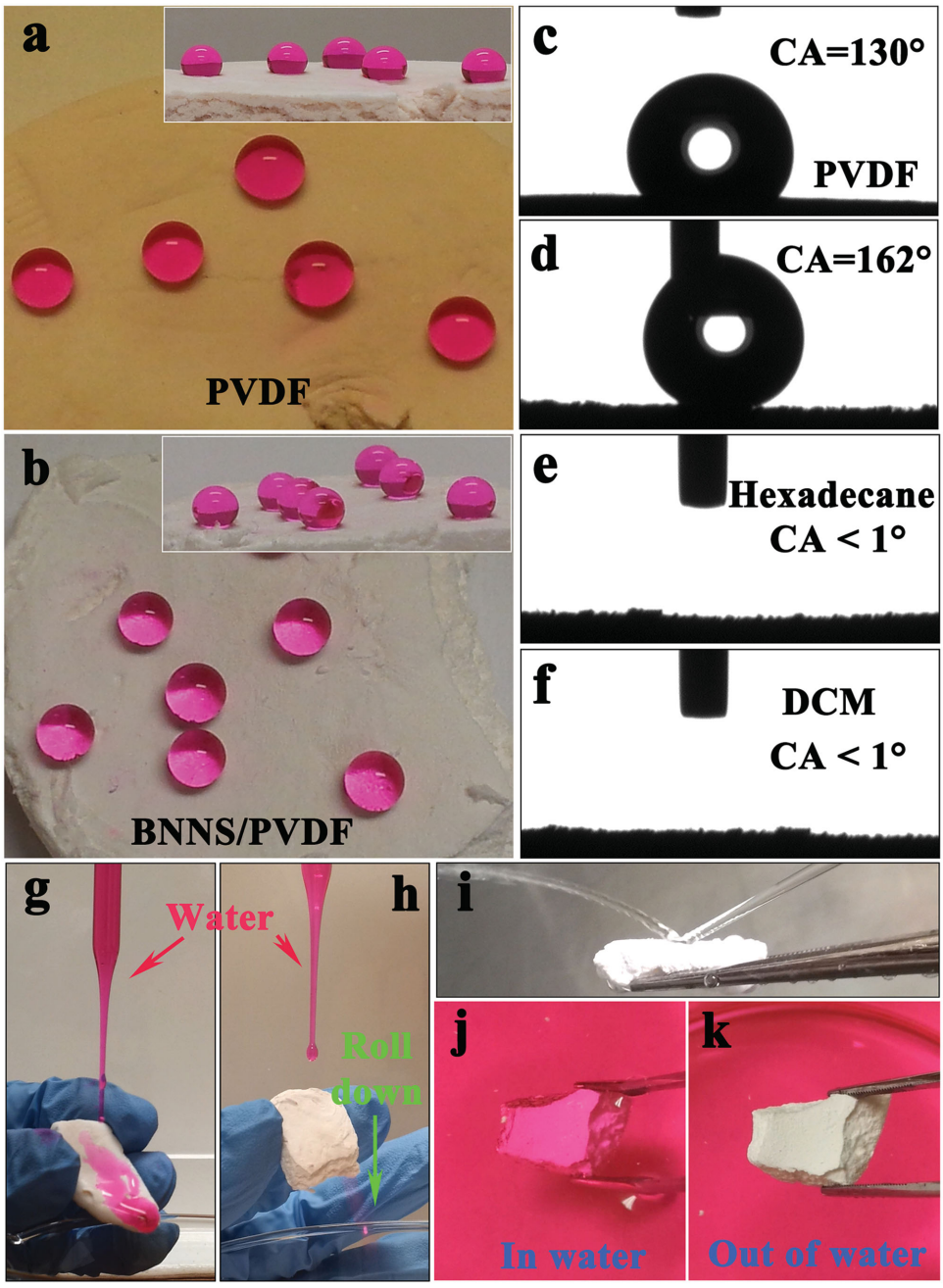

Figure 4. a,b) Photographs of water droplets (dyed red with rhodamine B) on the surfaces of the pure PVDF and porous BNNS/PVDF composite materials (inset: side views of the water droplets), respectively; c) the shape of a water droplet (6 μL) resting on the surface of pure PVDF; d) the shape of a water droplet (6 μL) on the surface of the porous BNNS/PVDF composite material showing a CA of 162°; e,f) the photographs of the oil (hexadecane and DCM) droplets on the surface of porous BNNS/PVDF composite material showing a nearly zero CA, respectively; g,h) photographs of water droplets drop down on the surface of the pure PVDF and porous BNNS/PVDF composite materials: water droplets will roll down rapidly from the surface of porous BNNS/PVDF composite material but be absorbed on the surface of pure PVDF; i) a jet of water bouncing on the surface of porous BNNS/PVDF composite material; and j, k) photographs of porous BNNS/PVDF composite material was immersed in and taken out from the water bath (I: immersed in water, II: taken out from water and no water adsorbed on the surface. water was dyed red with rhodamine B).

Figure 4 displays the wetting behaviors of water and oil on the surface of the pure PVDF and porous BNNS/PVDF composite materials. It is found that the pure PVDF is hydrophobic with a water CA of about 130° (Figure 4a,c) similar to that reported by Zha et al.[17] The addition of *h*-BNNSs can change the wettability of the PVDF from hydrophobic to superhydrophobic. Figure 4b displays several stationary water droplets (dyed red with rhodamine B) resting on the surface of the porous BNNS/PVDF composite material with a water CA of 160° (Figure 4d). Usually, the CA of a liquid droplet on a rough solid surface composed of air and solid can be estimated by the Cassie–Baxter equation[27]

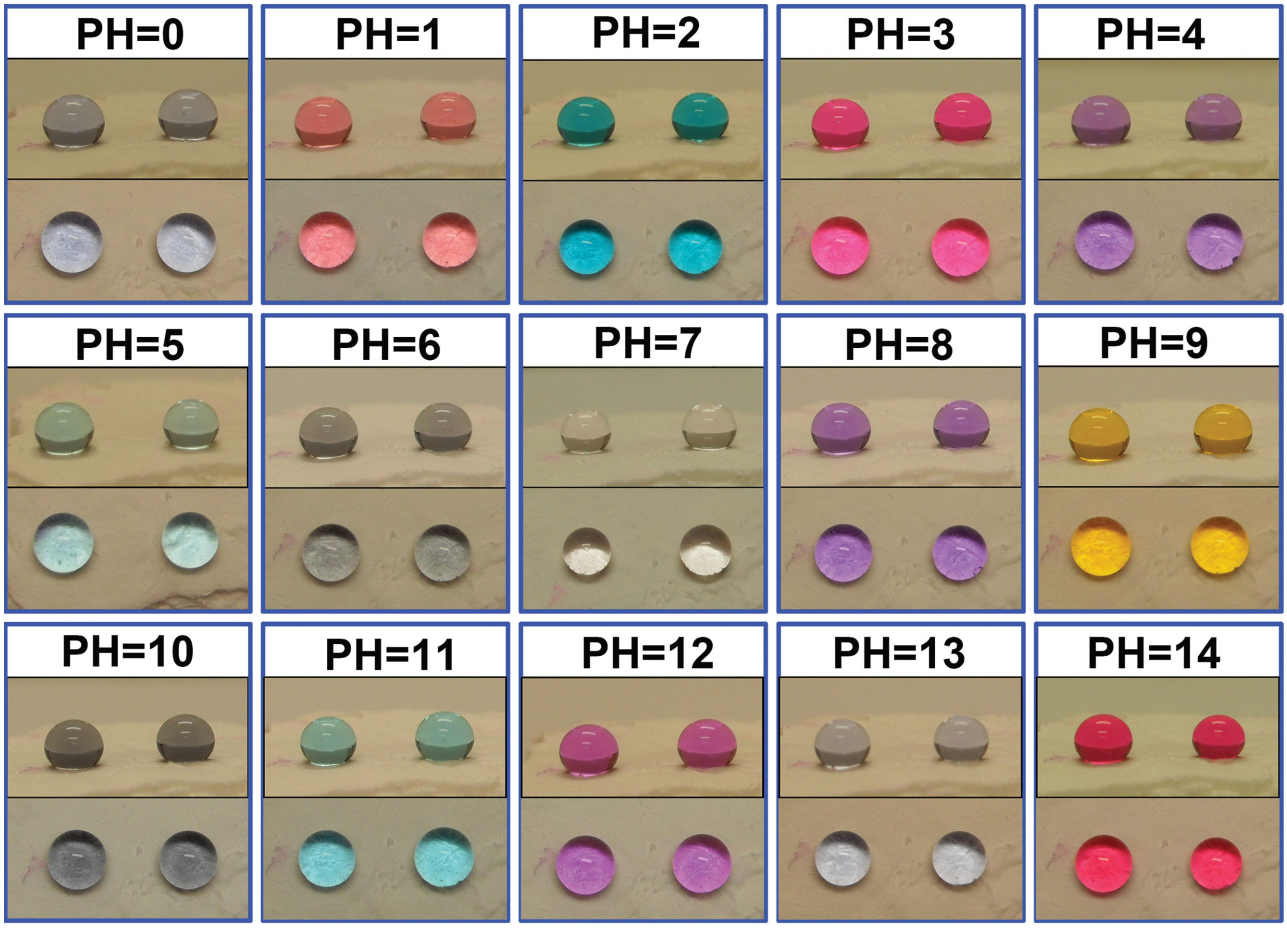

Figure 5. The photographs of the water droplets with different PH values (dyed with different color for visibility) on the surface of porous BNNS/PVDF (Insets are the corresponding side views of water droplets). Clearly, the change of the water CA with the variation of the PH value is very small, indicating good stability of the porous BNNS/PVDF composite materials in a wide PH range.

$$\cos\theta_r = f_1\cos\theta - f_2 \quad (1)$$

In Equation (1), θ_r and θ represent the CA obtained on a rough surface and on a smooth surface of the same material, respectively; f_1 and f_2 ($f_1 + f_2 = 1$) are the surface fractions corresponding to the proportion of the surface in contact with the water drop and the surface area in contact with trapped air, respectively. This equation suggests that increasing the fraction of air (f_2) will increase the CA of water droplets on the rough solid surface (θ_r). The water CA of hot-pressed PVDF dense membranes with a skin-layer is about 90° based on the previous reports.[28] Then, according to the Cassie–Baxter equation, the f_2 values of the pure porous PVDF and porous BNNS/PVDF composite materials are calculated to be about 0.643 and 0.940, respectively, meaning that about 64% and 94% of the contact area between the water droplet and the pure porous PVDF and porous BNNS/PVDF composite materials are occupied by air, respectively. Clearly, the introduction of a small amount of *h*-BNNSs can effectively increase the fraction of air (f_2) trapped between the water and porous BNNS/PVDF composite material. The results are in accordance with the FESEM analysis. The existence of a large amount of pores as well as the nanometer scale valleys formed by the loose nanoparticles (Figure 1f) and the spherical microparticles on the surface of porous BNNS/PVDF composite material could trap more air than that of the pure porous PVDF material. This thereby reduces the wettability of PVDF from hydrophilic to superhydrophobic.

Additionally, the porous BNNS/PVDF composite material exhibits a very small sliding angle (<3°), so that the water droplets can spontaneously roll off once the surface tilted. Figure 4h shows that water droplets run down the surface of the porous BNNS/PVDF composite material (Supporting Information Movie SI). Even a jet of water can bounce off the surface of the porous BNNS/PVDF composite material without leaving a trace (Figure 4i, Supporting Information Movie SII). In contrast, the water droplets adhere to the surface of the pure porous PVDF (Figure 4g, Supporting Information Movie SIII). Moreover, the nonwettability is uniform for the whole porous BNNS/PVDF composite material. Figure 4j,k shows that the porous BNNS/PVDF composite material is immersed in and taken out of the water bath (dyed red with rhodamine B). Clearly, the porous BNNS/PVDF composite material is completely dry after being taken out of the water (Supporting Information Movie SIV). In addition, the superhydrophobicity of the porous BNNS/PVDF composite material is stable over a wide pH range, as well as in some salt solutions. As shown in **Figure 5**, the water

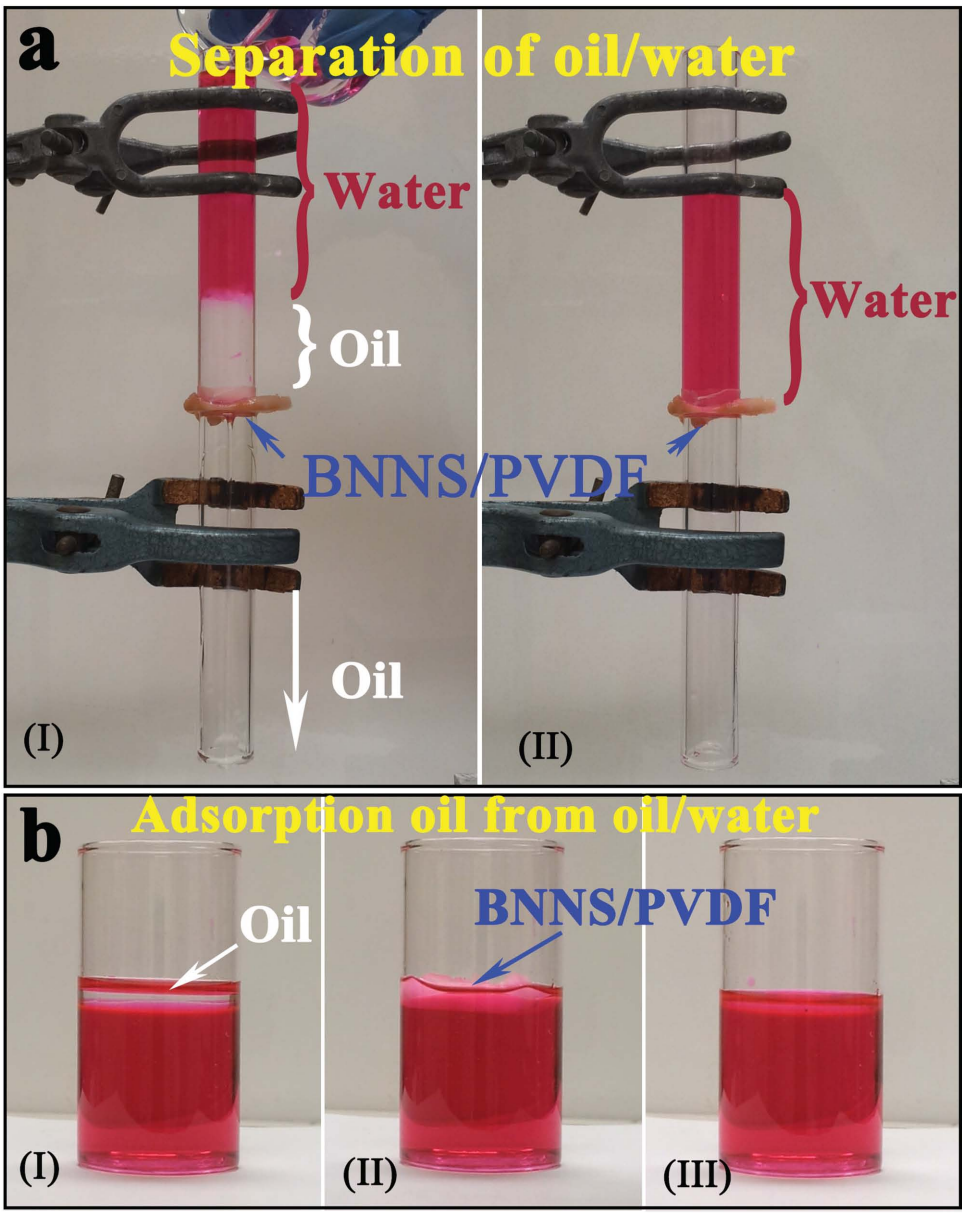

Figure 6. The experimental setup and the process of oil (DCM and *n*-hexane) filtering/adsorption: a) separation insoluble oil from water with the porous BNNS/PVDF composite material as filter membrane, oil can penetrate through porous BNNS/PVDF composite membrane and flow down rapidly (water is dyed red using rhodamine B for visibility), b) absorption of insoluble oil from water with the porous BNNS/PVDF composite material as absorbent and oil can be absorbed quickly by the porous BNNS/PVDF composite absorbent (Water is dyed red using rhodamine B for visibility).

droplets over a wide pH range from 0 to 14 can rest on the surfaces of the porous BNNS/PVDF composite material with high CAs over 150°. The wettability of a large number of salt solutions was also examined. Similarly, no obvious change in the water CAs was observed (Figure S6, Supporting Information). The results indicate that such porous BNNS/PVDF composite material can be employed in different conditions, including acidic, basic, and some salt solutions. Nevertheless, the addition of *h*-BNNSs does not alter the wettability of oil. As shown in Figure 4e,f, the oil droplets (exemplified via hexadecane and dichloromethane (DCM)) rapidly spread and penetrate into the porous BNNS/PVDF composite materials as soon as they are in contact with the surface of the composite materials.

Having characterized the porous BNNS/PVDF composite material and established that it exhibits superhydrophobic and superoleophilic properties we then examined whether it could efficiently separate or absorb insoluble oil from water. The separation process of oil from an oil/water mixture using the porous BNNS/PVDF composite material as the filter membrane is shown in **Figure 6**a (I and II). The porous BNNS/PVDF membrane was placed between two glass tubes, which were clamped together and sealed with PTFE tape. DCM was

selected as a model oil. It was found that DCM can easily pass through the porous superoleophilic BNNS/PVDF membrane, while water remains above the membrane because of its superhydrophobicity (Supporting Information Movie SV). More importantly, after separation, no water is observed in the oil or vice versa (Figure S7, Supporting Information), indicating highly effective separation of the oil from water. To test the stability of the porous BNNS/PVDF composite material, 20 cycles of the separation of DCM/water mixture was performed as displayed in **Figure 7**a. It can be seen that the flux of DCM decreases gradually with increasing cycle number but no sharp decline is observed. After 20 cycles, the flux remains at a relative high level of 2.653 L m^{-2} s^{-1}, which is 94% of the original flux (2.811 L m^{-2} s^{-1}, Supporting Information Movie SV).

The utilization of the porous BNNS/PVDF composite material as an oil/water absorption media was also investigated by testing the absorption–drying behavior with *n*-hexane as the model oil (Figure 6b (I–III), Supporting Information Movie SVI). Clearly, the porous BNNS/PVDF composite material showed stable performance over 20 repetitions: the absorbent can still absorb a mass of *n*-hexane about 3.3 times of its dry weight and no damage is observed (Figure 7b, Supporting Information Movie SVI). Also, the porous BNNS/PVDF composite material can absorb a range of oils and the absorbed weight of the oil mainly depends on its density as shown in Figure 7c. For the high-density oil, such as DCM, the porous BNNS/PVDF exhibits a stable absorption capacity of over 7.8 times of its weight after 20 cycles. Although, the sorption capacities of BNNS/PVDF composite is lower in comparison with the others, such as carbonaceous nanofiber hydrogels and Aerogels (Supporting Information Table S1), the properties of BNNS/PVDF composites, especially the stability as well as the small pore size, may make them a promising material for emulsified oil/water separation. The results of separation and adsorption experiments indicate an excellent stability of the porous BNNS/PVDF composite material, which is very important for practical applications.

In conclusion, a chemically stable porous BNNS/PVDF composite material with superhydrophobic and superoleophilic properties was fabricated by gelation and freeze-drying. Oil separation and absorption experiments demonstrate that such porous BNNS/PVDF composite materials can be efficiently used to clean the insoluble oil from water as either membranes or absorbents. More importantly, the composite material exhibits good stability, durability and antifouling features which match well with the requirements for treating oil-polluted water in practical applications.

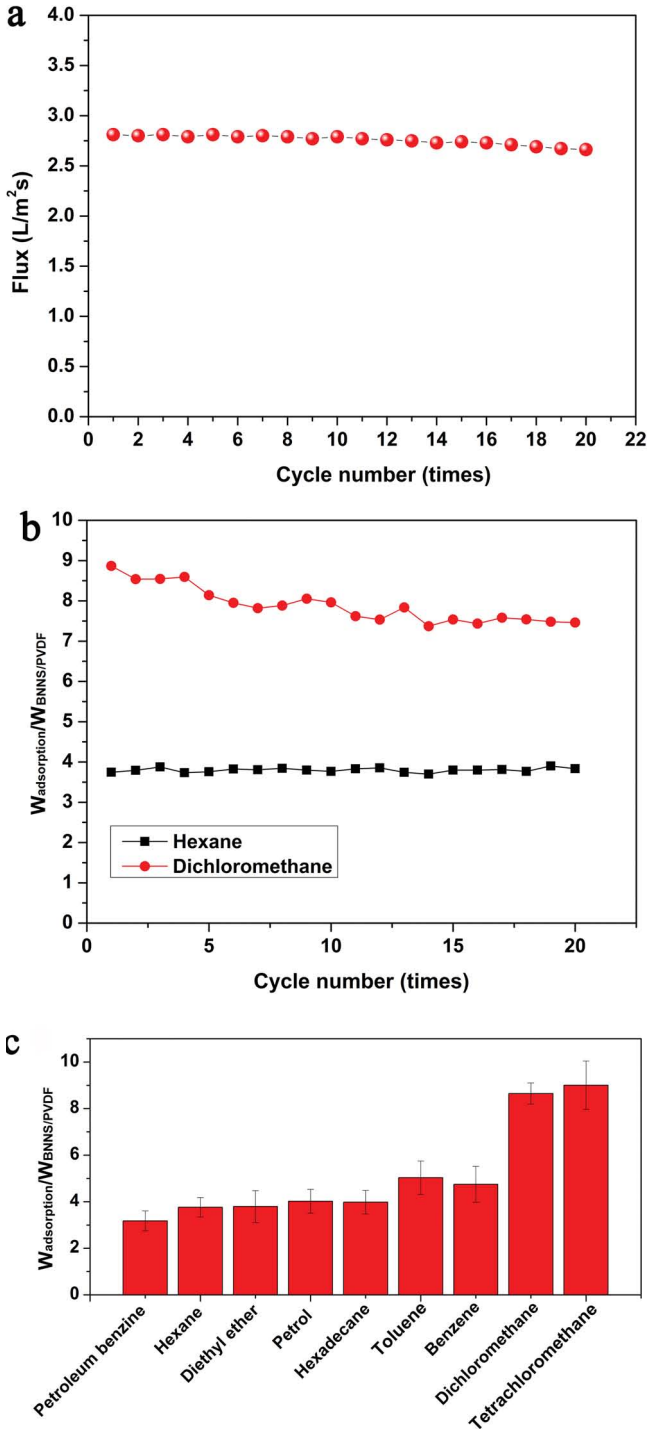

Figure 7. Study of the stability of the porous BNNS/PVDF composite material: a) change of the flux and decline rate of the DCM with increasing cycle number, and b) change of the absorbance and decline rate of the DCM and n-hexane with increasing cycle number. c) The absorption ratios of the porous BNNS/PVDF composite material for different oils.

Experimental Section

Preparation of h-BNNSs: In a typical exfoliation process, 1 g bulk *h*-BN powder was dispersed in 200 mL of IPA in a 250-mL conical flask. The solution was subjected to ultrasonication for 20 h in a low power ultrasonic bath. After ultrasonication, the supernatant was centrifuged at 1000 rpm for 20 min to remove the large unexfoliated *h*-BN particles. Then, the supernatant was further centrifuged at a higher rate of 10 000 rpm for 90 min, separating the small nanoparticles in the supernatant from the *h*-BNNSs in the sediment. Afterward, the sediment was collected and washed with ethanol several times to remove the IPA completely and dried at 60 °C for 1 h. Finally, the dried powder was used as the filler for porous BNNSs/PVDF composite material fabrication.

Preparation of Porous BNNS/PVDF Composite Material: In a typical process, 1 g PVDF (Mr = 20 000–30 000) was dissolved in 9 g DMF to form a homogeneous PVDF/DMF solution at 60 °C with stirring. After

cooling to room temperature, 50 mg of *h*-BNNSs were added into the PVDF/DMF solution and ultrasonicated to form a stable BNNS/PVDF/DMF suspension. The BNNS/PVDF/DMF suspension was placed in a closed container with a reservoir of methanol for 72 h. In this process, the methanol gradually volatilized and was absorbed by the BNNS/PVDF/DMF suspension. The BNNS/PVDF/DMF suspension gradually transformed into a gel via solvent exchange. The aged gel was then immersed into distilled water for another 4 d at room temperature to thoroughly remove the DMF. Then, the gel was frozen and dried at –40 °C (<0.2 mbar) for 20 h to form the dried porous material. The porous PVDF material without BNNSs was prepared by the same process.

Separation and Stability Tests of Porous BNNS/PVDF Utilized as a Separation Membrane: The oil/water mixtures were prepared by mixing water (dyed red with rhodamine B) and DCM with a volume ratio of 1:1 and strongly stirred for 10 min. The porous BNNS/PVDF composite material with the thickness of about 3 mm was selected to separate the oil/water mixture as a filter membrane. The membrane was placed between two glass tubes which were clamped together and sealed with PTFE tape. For every separation, a total of 100 mL of oil/water mixture was slowly poured into the glass tube, and separated by the porous BNNS/PVDF composite membrane. To test the stability of the porous BNNS/PVDF composite material, the separation experiment was repeated for 20 times. After each filtration, the porous BNNS/PVDF composite material was washed with ethanol and dried at 60 °C in air. The flux of the separated oil was calculated using

$$\text{Flux} = V / St$$

where V is the volume of oil filtered per unit of time (L), S is the projected area of the porous BNNS/PVDF membrane in contact with the oil/water mixture (m^2), and t is the filtration time (s).

Absorption and Stability Tests of Porous BNNS/PVDF Utilized as Absorbent: In a typical absorption process, a quantity of oil was absorbed by a certain quantity of porous BNNS/PVDF composite material. Then, the oil saturated porous BNNS/PVDF composite material was weighed using an electronic balance. To test the stability of the porous BNNS/PVDF composite material, the absorption experiment was repeated for 20 times. After weighing, the composite material was dried at 60 °C in air. The process was repeated and the weight of the oil saturated porous BNNS/PVDF composite material was measured each time. The absorbance of the oil was calculated with the following equation

$$R = W_{assorption} / W_{BNNS/PVDF}$$

where R is the ratio of weight (times), $W_{adsorption}$ is the weight of the oil absorbed by porous BNNS/PVDF composite material, and $W_{BNNS/PVDF}$ is the weight of dry porous BNNS/PVDF composite material.

Characterization: The morphology of the bulk *h*-BN, *h*-BNNSs, pure PVDF material, and porous BNNS/PVDF composite material was imaged using a Zeiss Ultra Plus FESEM. The surface characteristics and thickness of the *h*-BNNSs were examined using a Cypher AFM. A JEOL 2100F TEM was used to investigate the structure and thickness of the *h*-BNNSs. Fourier Transform Infrared spectroscopy (FTIR, Perkin Elmer) was used to identify bonding between boron and nitrogen and other elements. The surface wettability of the pure PVDF and porous BNNS/PVDF composite materials was characterized using a KSV CAM200 Goniometer instrument at ambient temperature in air. The CAs were determined by averaging measurements taken from at least five different positions on the measured surface.

Supporting Information

Supporting Information is available from the Wiley Online Library or from the author.

Acknowledgements

The authors acknowledge the financial supports from the Australian Microscopy and Microanalysis Research Facility (AMMRF) and from the Australian Research Council in the form of the Discovery Projects.

Received: June 3, 2014
Revised: September 26, 2014
Published online: November 3, 2014

[1] a) A. B. Nordvik, J. L. Simmons, K. R. Bitting, A. Lewis, T. Strom-Kristiansen, *Spill Sci. Technol. B* **1996**, *3*, 107; b) L. P. Gossen, L. M. Velichkina, *Pet. Chem.* **2006**, *46*, 67; c) M. A. Shannon, P. W. Bohn, M. Elimelech, J. G. Georgiadis, B. J. Marinas, A. M. Mayes, *Nature* **2008**, *452*, 301; d) P. Kajitvichyanukul, Y. T. Hung, L. K. Wang, *Handbook of Environmental Engineering: Advanced Physicochemical Treatment Processes* Vol. *4* (Eds: L. K. Wang, Y.-T. Hung, N. K. Shammas), The Humana Press Inc., Totowa, NJ **2006**, p. 521.

[2] a) D. Dudgeon, A. H. Arthington, M. O. Gessner, Z. Kawabata, D. J. Knowler, C. Leveque, R. J. Naiman, A. H. Prieur-Richard, D. Soto, M. L. J. Stiassny, C. A. Sullivan, *Biol. Rev.* **2006**, *81*, 163; b) C. Wu, C. Maurer, Y. Wang, S. Xue, D. L. Davis, *Environ. Health Perspect.* **1999**, *107*, 251.

[3] a) W. B. Zhang, Z. Shi, F. Zhang, X. Liu, J. Jin, L. Jiang, *Adv. Mater.* **2013**, *25*, 2071; b) W. W. Lei, D. Portehault, D. Liu, S. Qin, Y. Chen, *Nat. Commun.* **2013**, *4*, 1777; c) A. Bayat, S. F. Aghamiri, A. Moheb, G. R. Vakili-Nezhaad, *Chem. Eng. Technol.* **2005**, *28*, 1525; d) M. O. Adebajo, R. L. Frost, J. T. Kloprogge, O. Carmody, S. Kokot, *J. Porous. Mater.* **2003**, *10*, 159.

[4] Y. L. Yu, H. Chen, Y. Liu, V. S. J. Craig, L. H. Li, Y. Chen, A. Tricoli, *Polymer* **2014**, *55*, 5616.

[5] Y. L. Yu, H. Chen, Y. Liu, V. Craig, L. H. Li, Y. Chen, *Adv. Mater. Inter.* **2014**, *1*, 130002.

[6] C. G. Gao, Z. X. Sun, K. Li, Y. N. Chen, Y. Z. Cao, S. Y. Zhang, L. Feng, *Energy Environ. Sci.* **2013**, *6*, 1147.

[7] F. J. Wang, S. Lei, M. S. Xue, J. F. Ou, W. Li, *Langmuir* **2014**, *30*, 1281.

[8] G. Hayase, K. Kanamori, M. Fukuchi, H. Kaji, K. Nakanishi, *Angew. Chem Int. Ed.* **2013**, *52*, 1986.

[9] a) L. Feng, Z. Y. Zhang, Z. Y. Mai, Y. M. Ma, B. Q. Liu, L. Jiang, D. B. Zhu, *Angew. Chem Int. Ed.* **2004**, *43*, 2012; b) L. Feng, Z. Y. Zhang, Z. H. Mai, Y. M. Ma, B. Q. Liu, L. Jiang, D. B. Zhu, *Angew. Chem.* **2004**, *116*, 2046.

[10] J. P. Zhang, S. Seeger, *Adv. Funct. Mater.* **2011**, *21*, 4699.

[11] Y. L. Zhang, S. Wei, F. J. Liu, Y. C. Du, S. Liu, Y. Y. Ji, T. Yokoi, T. Tatsumi, F. S. Xiao, *Nano Today* **2009**, *4*, 135.

[12] a) T. Ono, T. Sugimoto, S. Shinkai, K. Sada, *Nat. Mater.* **2007**, *6*, 429; b) H. B. Sonmez, F. Wudl, *Macromolecules* **2005**, *38*, 1623.

[13] a) H. W. Liang, Q. F. Guan, L. F. Chen, Z. Zhu, W. J. Zhang, S. H. Yu, *Angew. Chem.* **2012**, *51*, 5101; b) H. P. Cong, X. C. Ren, P. Wang, S. H. Yu, *ACS Nano* **2012**, *6*, 2693; c) Z. Y. Wu, C. Li, H. W. Liang, J. F. Chen, S. H. Yu, *Angew. Chem Int. Ed.* **2013**, *52*, 2925; d) Z. Y. Wu, C. Li, H. W. Liang, Y. N. Zhang, X. Wang, J. F. Chen, S. H. Yu, *Scientific Reports*, *4*, 4079.

[14] J. Ge, Y. D. Ye, H. B. Yao, X. Zhu, X. Wang, L. Wu, J. L. Wang, H. Ding, N. Yong, L. H. He, S. H. Yu, *Angew. Chem Int. Ed.* **2014**, *53*, 3612.

[15] F. Liu, N. A. Hashim, Y. T. Liu, M. R. M. Abed, K. Li, *J. Membrane, Sci.* **2011**, *375*, 1.

[16] M. Peng, H. Li, L. Wu, Q. Zheng, Y. Chen, W. Gu, *J. Appl. Poly. Sci.* **2005**, *98*, 1358.

[17] D. Zha, S. Mei, Z. Wang, H. Li, Z. Shi, Z. Jin, *Carbon* **2011**, *49*, 5166.

[18] a) C. Li, Y. Bando, C. Zhi, Y. Huang, D. Golberg, *Nanotechnology* **2009**, *20*, 385707; b) T. Ouyang, Y. Chen, Y. Xie, K. Yang, Z. Bao, J. Zhong, *Nanotechnology* **2010**, *21*, 245701; c) C. Tang, Y. Bando, C. Liu, S. Fan, J. Zhang, X. Ding, D. Golberg, *J. Phys. Chem. B* **2006**, *110*, 10354.

[19] a) Y. Chen, J. Zou, S. J. Campbell, G. L. Caer, *Appl. Phys. Lett.* **2004**, *84*, 2430; b) R. Gao, L. Yin, C. Wang, Y. Qi, N. Lun, L. Zhang, Y. Liu, L. Kang, X. Wang, *J. Phys. Chem. C* **2009**, *113*, 15160; c) K. Watanabe, T. Taniguchi, H. Kanda, *Nat. Mater.* **2004**, *3*, 404; d) C. Y. Zhi, Y. Bando, C. C. Tang, Q. Huanga, D. Golberg, *J. Mater. Chem.* **2008**, *18*, 3900; e) H. Chen, Y. Chen, Y. Liu, C. N. Xu, J. S. Williams, *Optical Mater.* **2007**, *29*, 1295; f) H. Chen, Y. Chen, Y. Liu, L. Fu, C. Huang, D. Llewellyn, *Chem. Phys. Lett.* **2008**, *463*, 130.

[20] D. Golberg, Y. Bando, C. Tang, C. Zhi, *Adv. Mater.* **2007**, *19*, 2413.

[21] X. B. Wang, Q. H. Weng, X. Wang, X. Li, J. Zhang, F. Liu, X. F. Jiang, H. X. Guo, N. S. Xu, D. Golberg, Y. Bando, *ACS Nano.*, *5*, 9081.

[22] a) G. E. Padawer, N. Beecher, *Polym. Eng. Sci.* **1970**, *10*, 185; b) P. May, U. Khan, A. O'Neill, J. N. Coleman, *J. Mater. Chem.* **2012**, *22*, 1278.

[23] U. Khan, P. May, A. O'Neill, A. P. Bell, E. Boussac, A. Martin, J. Semple, J. N. Coleman, *Nanoscale* **2013**, *5*, 581.

[24] Y. F. Xue, Q. Liu, G. He, K. Xu, L. Jiang, X. Hu, J. Hu, *Nanoscale Res. Lett.* **2013**, *8*, 49.

[25] J. M. Guenet, *Thermoreversible Gelation of Polymers and Biopolymers* Academic Press, London **1992**.

[26] X. B. Wang, A. Pakdel, J. Zhang, Q. H. Weng, T. Y. Zhai, C. Y. Zhi, D. Golberg, Y. Bando, *Nanoscale Res. Lett.* **2012**, *7*, 662.

[27] A. B. D. Cassie, S. Baxter, *Trans. Faraday Soc.* **1944**, *40*, 546.

[28] J. F. Hester, P. Banerjee, Y. Y. Won, A. Akthakul, M. H. Acar, A. M. Mayes, *Macromolecules* **2002**, *35*, 7652.